Theory of the structure of electronic polarization and its strain dependence in ferroelectric perovskites

Yanpeng Yao and Huaxiang Fu
Department of Physics, University of Arkansas, Fayetteville, Arkansas 72701, USA
(Received 8 August 2008; revised manuscript received 21 October 2008; published 6 January 2009)

The $\phi(\vec{k}_\perp)\sim\vec{k}_\perp$ relation is called polarization structure, describing the Berry's phase contribution $\phi(\vec{k}_\perp)$ to the electronic polarization from individual $\vec{k}_\perp$ points that are on the Brillouin-zone plane perpendicular to the direction of polarization. By density-functional calculations, we study the polarization structure in ferroelectric perovskite $PbTiO_3$, revealing (i) the $\vec{k}_\perp$ point that contributes most to the electronic polarization, (ii) the magnitude of bandwidth, and (iii) subtle curvature of polarization dispersion. We also investigate how polarization structure in $PbTiO_3$ is modified by compressive in-plane strains. The bandwidth of polarization dispersion in $PbTiO_3$ is shown to exhibit an unusual decline although the total polarization is enhanced. As another outcome of this study, we formulate an analytical scheme for the purpose of identifying what determines the polarization structure at arbitrary $\vec{k}_\perp$ points by means of the Wannier functions. We find that $\phi(\vec{k}_\perp)$ is determined by two competing factors: one is the overlaps between the neighboring Wannier functions within the plane *perpendicular* to the polarization direction and the other is the localization length *parallel* to the polarization direction. In-plane strain increases the former while decreases the latter, causing interesting nonmonotonous effects on polarization structure. Finally, polarization dispersion in another paradigm ferroelectric $BaTiO_3$ is discussed and compared with that of $PbTiO_3$.

DOI: 10.1103/PhysRevB.79.014103 PACS number(s): 77.22.Ej, 77.80.−e

I. INTRODUCTION

Electric polarization is a key quantity for computing and understanding technologically relevant effective charges, dielectric, and piezoelectric responses that are the derivatives of polarization with respect to atomic displacement, electric field, and strain, respectively.[1] Polarization also plays an important role in the methodology development of the theory dealing with finite electric fields in infinite solids by minimization of the free energy $F=U-\vec{E}\cdot\vec{P}$.[2–5] Total electric polarization consists of electronic contribution ($\vec{P}_{\rm el}$) and ionic component ($\vec{P}_{\rm ion}$). Computing the latter component is straightforward using point charges, while calculating the electronic polarization is not. Today $\vec{P}_{\rm el}$ is calculated using the sophisticated modern theory of polarization.[6,7] According to the theory, $\vec{P}_{\rm el}$ corresponds to a geometrical phase of the valence electron states,

$$\vec{P}_{\rm el}=\frac{2e}{(2\pi)^3}\int d\vec{k}_\perp\phi(\vec{k}_\perp), \tag{1}$$

where

$$\phi(\vec{k}_\perp)=i\sum_{n=1}^{M}\int_0^{G_\parallel}d\vec{k}_\parallel\left\langle u_{n\vec{k}}\left|\frac{\partial}{\partial k_\parallel}\right|u_{n\vec{k}}\right\rangle \tag{2}$$

is the Berry phase of occupied Bloch wave functions $u_{n\vec{k}}$. Subscripts $\parallel$ and $\perp$ mean parallel and perpendicular to the polarization direction, respectively. Practically, to carry out the $\vec{P}_{\rm el}$ calculations, the integral in Eq. (1) is replaced by a weighted summation of the phases at sampled discrete $\vec{k}$ points (Monkhorst-Pack scheme,[8] for example) in the two-dimensional (2D) $\vec{k}_\perp$ plane, namely, $\vec{P}_{\rm el}=\Sigma_{\vec{k}_\perp}\omega(\vec{k}_\perp)\phi(\vec{k}_\perp)$, with weight $\Sigma_{\vec{k}_\perp}\omega(\vec{k}_\perp)=1$. The polarization at individual $\vec{k}_\perp$, $\phi(\vec{k}_\perp)$, is calculated as the phase of the determinant formed by valence states at two neighboring $\vec{k}$'s on the $\vec{k}_\parallel$ string as[6,7]

$$\phi(\vec{k}_\perp)=\mathrm{Im}\left\{\ln\prod_{j=0}^{J-1}\det(\langle u_{k_j,m}|u_{k_{j+1},n}\rangle)\right\}. \tag{3}$$

Defined as such, the total polarization $\vec{P}=\vec{P}_{\rm ion}+\vec{P}_{\rm el}$ could be uniquely determined and gauge independent up to a modulus constant. In Eq. (1) one sees that it is the $\phi(\vec{k}_\perp)$ phases at different $\vec{k}_\perp$ that determine the electronic polarization. The purpose of this work is to study the properties of $\phi(\vec{k}_\perp)$.

The physical significance of the $\phi(\vec{k}_\perp)$ quantity can be understood by analogy. It is well known that band structure, which describes the relation between single-particle orbital energy and electron wave vector $\vec{k}$, is very useful for understanding electronic, photoexcitation, and photoemission properties in solids.[9] The $\phi(\vec{k}_\perp)\sim\vec{k}_\perp$ relation may be similarly termed as "polarization structure" or "polarization-phase structure." Electron states in band structure can be changed by photoexcitation or emission. The $\vec{k}_\perp$-point polarization phase can be altered by electric fields, which act as a possible excitation source for electrical polarization. Note that electrical fields do not alter the electron wave vector ($\vec{k}_\perp$) perpendicular to the direction of the field, and thus $\vec{k}_\perp$ remains a conserved quantity. The field-induced variation in $\phi(\vec{k}_\perp)$ in fact manifests the $\vec{k}_\perp$-dependent polarization current. As a result, the relevance of polarization structure to electronic polarization is similar to the band structure to electronic properties.

Furthermore, understanding the $\phi(\vec{k}_\perp)$ quantity is of useful value from both fundamental and computational points of views. Fundamentally, this quantity is determined by the Bloch wave functions, not in the ordinary sense of spatial

distribution but through the interesting aspects of the Berry's phase of occupied manifold of electron states. Studying how $\phi(\vec{k}_\perp)$ depends on $\vec{k}_\perp$ may yield better understanding of electron states, as well as the rather intriguing connection between these states and their contributions to polarization in insulator solids. Computationally, we first recognize that the $\phi(\vec{k}_\perp)$ phase computed from Eq. (3) always produces a value within the principal range $[0,2\pi]$. In reality, depending on the dispersion of $\phi(\vec{k}_\perp)$ as a function of $\vec{k}_\perp$, it is possible that the phases for different $\vec{k}$ points fall in different branches. In other words, the true $\phi(\vec{k}_\perp)$ values may fall in the principal range for some $\vec{k}_\perp$ points (let us denote this set of $\vec{k}_\perp$ points as $\vec{k}_\perp^{(\mathrm{I})}$) while falling out of the principal range for other $\vec{k}_\perp$ (to be denoted as $\vec{k}_\perp^{(\mathrm{II})}$). We find numerically that this indeed happens for real materials particularly when polarization is large; a specific example is given in Sec. II. When this occurs, one must *not* artificially shift the phases of the $\vec{k}_\perp^{(\mathrm{II})}$ into the principal range, as computers do according to Eq. (3). Although this shift makes no difference to the polarization phase of individual $\vec{k}_\perp$ points, it will alter the total $\vec{P}_{\mathrm{el}}$ polarization, yielding spurious magnitude of polarization. Only when the phase of *every* $\vec{k}_\perp$ is shifted by a constant 2π will the total $\vec{P}_{\mathrm{el}}$ polarization remain equivalent. To find out which $\vec{k}_\perp$ may generate a phase not in the principal range, one in principle should compute the whole dispersion structure of polarization and then map out the $\phi(\vec{k}_\perp)$ for all $\vec{k}_\perp$ points based on the assumption that the $\phi(\vec{k}_\perp)$ phase is a continuous function of wave vector $\vec{k}_\perp$, which makes it important to study the properties of the $\phi(\vec{k}_\perp)$ phase as a function of $\vec{k}_\perp$.

Despite the relevance, the dispersion structure of polarization is nevertheless not completely understood. More specifically, (i) little is known about what determine the $\phi(\vec{k}_\perp)$ phase at individual $\vec{k}_\perp$. In Eq. (3), $\phi(\vec{k}_\perp)$ is determined by the wave functions of a string of $\vec{k}_\parallel$ points, not just a single $\vec{k}$. As a result, the answer to the question is highly nontrivial. (ii) For a given ferroelectric substance (say, the prototypical $PbTiO_3$), it is not clear which $\vec{k}_\perp$ exhibits the largest polarization contribution. Does the Γ point always contribute most or least? (iii) We do not know if the Berry's phases at different $\vec{k}_\perp$s share a similar value or are very different from each other, that is, a problem concerning the dispersion width of the polarization structure. Slightly more intriguing, one may wonder along which direction the $\phi \sim \vec{k}_\perp$ curve shows the largest dispersion. (iv) Even for two commonly studied ferroelectrics, $BaTiO_3$ and $PbTiO_3$, we do not know how different or similar their polarization structures are.

Recently, there is another active field in the study of polarization, which concerns the use of in-plane strain to tune the ferroelectric polarization.[10–14] This tunability stems from the fundamental interest in the strain-polarization coupling. Imposed under in-plane strain ferroelectrics subject to modifications of chemical bonds and/or charge transfer, thereby the interaction between atoms is altered. It has been known that a compressive in-plane strain tends to enhance the total polarization. But the amplitude of enhancement was found to be highly material dependent.[12,13] Furthermore, an interesting possibility of using biaxial tetragonal strain on the (001) plane to rotate the polarization of the rhombohedral phase was demonstrated in $BiFeO_3$ thin films, and large strain tuning of polarization was achieved.[14] Considering the importance of the strain effects, one might want to know how the $\phi(\vec{k}_\perp)$ phase from each $\vec{k}_\perp$ can be influenced by strain. Strain effects on the polarization dispersion remain largely unknown, however. It would be of interest to examine how the strain may tune and modify the dispersion of polarization structure. Specific questions on this aspect are: in what manner would the in-plane strain change the relative contributions and curvatures at different $\vec{k}_\perp$, and how the band width of the dispersion curve is to be altered?

With these questions in mind, we here study the dispersion structure of the polarization in ferroelectric perovskites, as well as its dependence on in-plane strains. Two complementary approaches (first-principles density-functional calculations and analytical formulations) are used. By means of analytical formulation, we aim at a better understanding on what specific quantities and/or interactions determine the polarization at individual $\vec{k}_\perp$ point. Our calculations reveal some useful knowledge on the polarization structure in perovskite ferroelectrics. For example, the largest $\phi(\vec{k}_\perp)$ contribution is shown not to come from the zone center but from the zone boundary. We also find that the polarization curve in $PbTiO_3$ is notably flat along the Γ-X_1 direction, and exhibits, however, a strong dispersion along the Γ-X_2 axis. Our theoretical analysis further reveals that the flat dispersion along the Γ-X_1 direction is caused by a small amount of participation from the nearest-neighbor interaction between the Wannier functions (WFs). Finally, the present study also demonstrates some rather interesting differences in $PbTiO_3$ and $BaTiO_3$, in terms of the polarization structures as well as their strain dependences.

II. POLARIZATION STRUCTURE OF LEAD TITANATE

We first present the density-functional calculations on the polarization structure in $PbTiO_3$. In its ferroelectric phase $PbTiO_3$ is tetragonal ($|\mathbf{a}_1|=|\mathbf{a}_2|=a, |\mathbf{a}_3|=c$) and possesses a large spontaneous polarization. The polarization is along the c-axis direction, perpendicular to the $\vec{k}_\perp$ plane. Calculations are performed within the local-density approximation (LDA).[15] We use pseudopotential method with mixed basis set.[16] The Troullier-Martins type of pseudopotentials are employed.[17] Details for generating pseudopotentials, including atomic configurations, pseudo/all-electron matching radii, and accuracy checking, were described elsewhere.[18] The energy cutoff is 100 Ry, which is sufficient for convergence. The calculations are performed in two steps: the optimized cell structure and atomic positions are first determined by minimizing the total energy and the Hellmann-Feynman forces, and after the structural optimization, the polarization dispersion of $\phi(\vec{k}_\perp)$ is calculated using the modern theory of polarization.[6,7] Our LDA-calculated in-plane lattice constant for unstrained $PbTiO_3$ (PT) is $a=3.88$ Å, with $c/a=1.04$, both agreeing well with other existing calculations.

Figure 1(a) shows the reduced 2D Brillouin zone (BZ) that the $\vec{k}_\perp$ points sample over. The calculated ϕ phases at

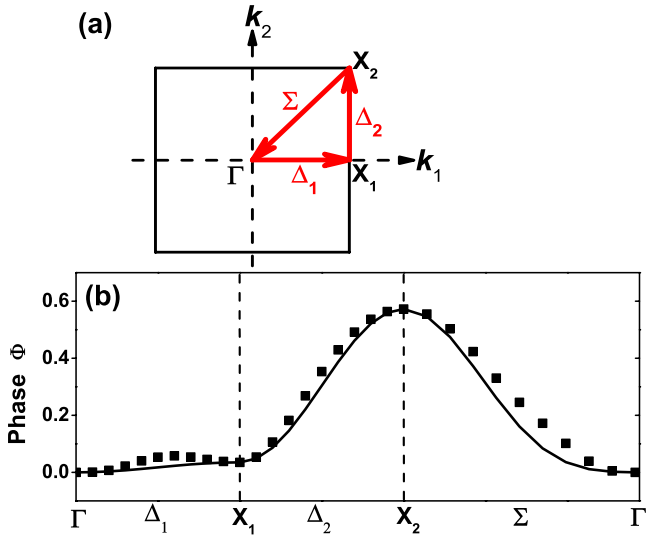

FIG. 1. (Color online) (a) The 2D Brillouin zone for the $\vec{k}_\perp$ plane; (b) Berry's phase at different $\vec{k}_\perp$ points for $PbTiO_3$ at equilibrium (symbols: direct calculation results; curve: analytical results). The $\phi(\vec{k}_\perp)$ phase is in units of rad.

individual $\vec{k}_\perp$ points along the $\Gamma \to X_1 \to X_2 \to \Gamma$ path are given in Fig. 1(b). Reciprocal-space coordinates of X_1 and X_2 are $\vec{k}_\perp = (\pi/a, 0)$ and $(\pi/a, \pi/a)$, respectively. The dispersion curve is rigidly shifted such that the phase at Γ is taken as the zero reference.

Before we discuss the specific results in Fig. 1, we need to point out that the shape of this $\vec{k}_\perp$-dependent phase curve is translation invariant. As is known, the electronic polarization alone can be an arbitrary value if the solid is uniformly translated with respect to a fixed origin of coordinates. Although different translations will change the absolute location of the polarization-dispersion curve, the shape of the curve remains unaffected, however. This can be easily illustrated by analyzing the change in the $\phi(\vec{k}_\perp)$ phase when one displaces the solid arbitrarily. Let the wave function of the original system be $\psi_{n\vec{k}}(\vec{r}) = e^{i\vec{k}\cdot\vec{r}} u_{n\vec{k}}(\vec{r})$, where $u_{n\vec{k}}(\vec{r}) = u_{n\vec{k}}(\vec{r}+\vec{R})$. Now, we displace the solid by an arbitrary vector $\vec{r}_0$, while the origin of coordinates is fixed. Let us denote the original system using script A and the displaced system using script B, so $\vec{r}_B = \vec{r}_A + \vec{r}_0$. The wave functions of the displaced system satisfy

$$\psi^B_{n\vec{k}}(\vec{r}_B) = \psi^A_{n\vec{k}}(\vec{r}_A) = \psi^A_{n\vec{k}}(\vec{r}_B - \vec{r}_0). \tag{4}$$

Thus we have $u^B_{n\vec{k}}(\vec{r}_B) = e^{-i\vec{k}\cdot\vec{r}_0} u^A_{n\vec{k}}(\vec{r}_B - \vec{r}_0)$. Substituting this relation into Eq. (2) or (3), one can obtain that the $\phi(\vec{k}_\perp)$ of the displaced system is

$$\phi^B(\vec{k}_\perp) = \phi^A(\vec{k}_\perp) + \vec{r}_0 \cdot \vec{G}_\parallel N^{\text{occ}}_{\text{band}}, \tag{5}$$

where $N^{\text{occ}}_{\text{band}} = M$ is the number of bands occupied by electrons. The phase differences between the A and B systems are thus a constant, independent of $\vec{k}_\perp$.

Several observations are ready in Fig. 1(b). (i) The largest $\phi(\vec{k}_\perp)$ polarization does not come from the zone-center Γ point. Rather surprisingly, the largest $\phi(\vec{k}_\perp)$ phase is from the X_2 point which lies at the far end of the BZ. (ii) The polarization curve is flat along the Γ-X_1 line showing only a small dispersion. On the other hand, the dispersion becomes very large along the Γ-X_2 direction. (iii) At $\vec{k}_\perp$ points of high symmetry (such as Γ, X_1, or X_2), the curve in Fig. 1(b) has zero slope, similar to the electron band structure. (iv) The dispersion of polarization also shows subtle details which could not be easily understood. For example, there is a local (although not very pronounced) maximum along the Δ_1 line, making the X_1 point a local minimum in both Γ-X_1 and X_1-X_2 directions.

Our calculations further reveal that despite the fact that the polarization in Fig. 1(b) exhibits substantial $\vec{k}_\perp$ dependency, the dispersion width ($\sim$0.6) is much smaller than 2π. This finding is important for the following reason. As described in Sec. I, if the differences of the $\phi(\vec{k}_\perp)$ phases at different $\vec{k}_\perp$ points are greater than 2π, one would encounter a difficulty in determining which branch of phase a specific $\vec{k}_\perp$ point should be assigned. This difficulty can be avoided only after the phases of all $\vec{k}_\perp$ points are mapped out. Fortunately, the result in Fig. 1(b) tells us that the phase contributions from different $\vec{k}_\perp$ points are fairly close, and the differences are far less than the critical value of 2π that may cause the above difficulty. Nevertheless, we should point out that even a small polarization dispersion as in Fig. 1(b) may still give rise to spurious results on total polarization. To illustrate this, we displace all five atoms in $PbTiO_3$ along the polar c axis by a distance z_0. Figure 2(a) shows the total (electronic+ionic) polarization, computed from the geometric phase, as a function of the displacement z_0 (in unit of c). Intuition tells us that the total polarization should be uniquely determined and translationally invariant. However, we see in Fig. 2(a) that unphysical discontinuity happens for some z_0 points, and this discontinuity shows up periodically. To understand what causes the discontinuity, we examine the phase contributions from individual $\vec{k}_\perp$ (sampled according to the Monkhorst-Pack scheme[8]), as depicted in Fig. 2(b). Figure 2(b) shows that the individual-$\vec{k}_\perp$ phases indeed are a periodic function of z_0, explaining why the discontinuity in Fig. 2(a) is periodic. Here it may be useful to comment briefly on the length of the periodicity. One might think that by displacing the solid by a distance of c in the c-axis direction, the $\phi(\vec{k}_\perp)$ phase would change by a value of 2π. However, the periodicity in Fig. 2 is much smaller than c. The explanation is simple. As a matter of fact, in real space the individual $\phi(\vec{k}_\perp)$ has a periodicity of $\frac{1}{N^{\text{occ}}_{\text{band}}} c$ (instead of c), which for $PbTiO_3$ the periodicity is $0.0455c$ because $N^{\text{occ}}_{\text{band}} = 22$. This is indeed consistent with the numerical calculation in PT [Fig. 2(b)]. The length of periodicity can be seen from Eq. (5) showing that whenever $\vec{r}_0 = \frac{n}{N^{\text{occ}}_{\text{band}}} \vec{R}_\parallel$ (n is an arbitrary integer and $\vec{R}_\parallel$ is the lattice vector along the $\vec{G}_\parallel$ direction), the $\phi^B(\vec{k}_\perp)$ and $\phi^A(\vec{k}_\perp)$ differ by $\phi^B(\vec{k}_\perp) = \phi^A(\vec{k}_\perp) + 2\pi n$. Figure 2(b) also reveals the reason responsible for the discontinuity of the total polarization. Spurious discontinuity occurs when the $\phi(\vec{k}_\perp)$ phases of some (but not all) individual $\vec{k}_\perp$ exceed 2π [Fig. 2(b)]. Under this situation, computers incorrectly shift the phases of these $\vec{k}_\perp$ points back to the principle

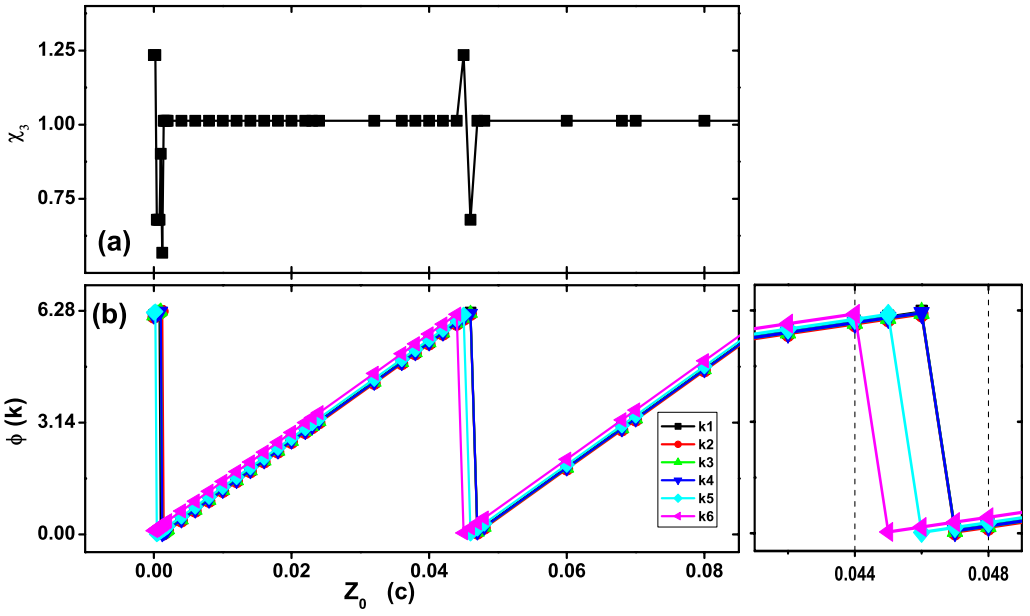

FIG. 2. (Color online) (a) Total polarization in strained $PbTiO_3$ of in-plane lattice constant $a=3.72$ Å as a function of the uniform displacement z_0 of five atoms; (b) the $\phi(\vec{k}_\perp)$ phases at six Monkhorst-Pack sampling $\vec{k}_\perp$ points as a function of z_0. For each $c/N_{\text{band}}^{\text{occ}}$ change in z_0, the $\phi(\vec{k}_\perp)$ phases change by 2π. In (b), the $\phi(\vec{k}_\perp)$ phase curves are enlarged in the right side of the figure for z_0 between 0.044 and 0.048.

range, yielding spurious total polarization. According to our experience, spurious polarization often takes place in two circumstances: one is for materials of very large polarization, such as tetragonal $BiScO_3$, and another is when atoms in the unit cell are translationally shifted. Given the small bandwidth of the $\phi(\vec{k}_\perp)$ dispersion, it is now straightforward that by using different $\vec{r}_0$'s, we can avoid the spurious polarization. However for some materials, if the dispersion width from different $\vec{k}_\perp$ points is larger than 2π, one may have to rely on the continuity of the $\phi(\vec{k}_\perp)$ phases and map out the phases of individual $\vec{k}_\perp$ points over the whole two-dimensional $\vec{k}_\perp$ plane in order to find the correct phase branch.

III. STRAIN DEPENDENCE OF POLARIZATION STRUCTURE

An important property of ferroelectrics is that the polarization is strongly dependent on strain. While strain can change the total polarization, response of the polarization-dispersion structure to strain could also be an interesting problem. This interest arises from the fact that the $\phi(\vec{k}_\perp)$ phases at different $\vec{k}_\perp$ may depend on in-plane strain very differently, manifesting the microscopic interactions between atoms along both the in-plane and out-of-plane directions. This microscopic knowledge is, however, lost in the total electronic polarization after the $\phi(\vec{k}_\perp)$ phases of different $\vec{k}_\perp$ points are integrated. Here we investigate the response of the polarization structure under in-plane strain in $PbTiO_3$. For each in-plane (a) lattice constant, the out-of-plane c lattice constant and atomic positions are fully relaxed by minimizing the DFT total energy. The polarization structure is then determined using the optimal structure.

Figure 3 shows the phase dispersion curves for $PbTiO_3$ at different in-plane lattice constants. All curves are shifted so that the phase at Γ point is zero in order to conduct direct comparison. Three conclusions can be drawn from Fig. 3. (i) The relative phase, $\phi(\vec{k}_\perp)-\phi(\Gamma)$, changes drastically for X_2 but not so significantly for X_1. (ii) At increasing strain, (or smaller in-plane a constant), the bandwidth of the dispersion initially changes very little when $a=3.84$ Å, and then starts to *decrease* upon further increasing strain to $a=3.80$ Å. The decline of the dispersion bandwidth is rather surprising since a compressive in-plane strain is known to enhance the total polarization in PT (which is given in the inset of Fig. 3). The decline is also counterintuitive when one considers that the decreasing in-plane lattice constant makes the atom-atom coupling stronger within the in-plane directions and should therefore have increased the bandwidth. One possible reason that may cause the decrease in the bandwidth is given in Sec. IV. As a result of the declining dispersion, the polarization curve becomes notably "flat" at small $a=3.65$ Å. (iii) The curvature of the dispersion also shows subtle changes, featured by the fact that a new dispersion minimum appears along the X_2-Γ line at large strain. As a consequence, the dispersion curvature [i.e., the second derivative $\nabla^2_{\vec{k}_\perp} P(\vec{k}_\perp)$] at Γ point alters its sign from being positive (at large a) to negative (at small a). Furthermore, the local maximum between Γ-X_1 for unstrained PT turns into a new minimum at large in-plane strains. Meanwhile, the X_1 point changes from a minimum into a saddle point when strain increases.

The calculations thus reveal that while in-plane strain has been previously known to introduce interesting modifications (sometimes markedly enlarged[12] and sometimes remarkably small[13]) to the *total* c-axis polarization, its effects on the polarization dispersion at individual $\vec{k}_\perp$ points appear to be

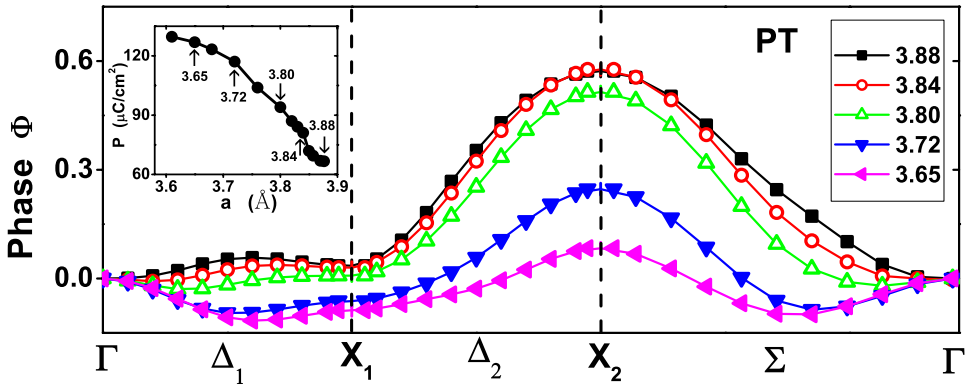

FIG. 3. (Color online) The ϕ phases of different $\vec{k}_\perp$ points for $PbTiO_3$ under different in-plane lattice constants. The inset shows the total polarization in $PbTiO_3$ as a function of in-plane lattice constant. Symbols are direct calculation results and curves are guides for the eyes.

even richer, showing that the polarization structure indeed is worth studying. The subtle response of the polarization structure, as predicted above, indicate that there is new and rather complex physics behind the results in Fig. 3. While we know that the strain-induced changes in the polarization dispersion must be associated with the fundamental modification of electron wave functions, we also have to admit that the DFT results obtained in our numerical calculations are puzzling, and an intuitive understanding of the results is difficult for two reasons. First, this is an early attempt to investigate the polarization structure, and there is not much previous understanding in the literature. Second, although Eqs. (2) and (3) allow us to compute precisely the polarization of individual $\vec{k}_\perp$, a direct and more intuitive connection between $\phi(\vec{k}_\perp)$ and Bloch wave functions is hard to capture from these equations. As a result, it would be very helpful if one could find an alternative way to understand the polarization structure and the computation results. For instance, what determines the polarization at individual $\vec{k}_\perp$ point and why $\phi(\vec{k}_\perp)$ maximizes at the X_2 point? In Sec. IV, we attempt a scheme which we wish to be able to offer a more intuitive understanding of the polarization structure.

IV. WANNIER FUNCTION FORMULATION OF POLARIZATION STRUCTURE

As mentioned above, Eqs. (2) and (3) give us little intuitive sense on the direct $\vec{k}_\perp$ dependence of the Berry's phase. In order to get more insight, we use the Wannier functions to analyze the polarization structure. Previously, the Wannier functions have been found very useful in analyzing real-space local polarization.[19,20] Here we employ the Wannier-function approach for a different purpose, namely, to understand the $\vec{k}_\perp$ dependence of the polarization structure. The Wannier functions are defined as

$$W_n(\vec{r}-\vec{R}) = \frac{\sqrt{N}\Omega}{(2\pi)^3}\int_{\mathrm{BZ}} d\vec{k} e^{i\vec{k}\cdot(\vec{r}-\vec{R})} u_{nk}(\vec{r}) \tag{6}$$

or

$$u_{nk}(\vec{r}) = \frac{1}{\sqrt{N}}\sum_{\vec{R}} e^{-i\vec{k}\cdot(\vec{r}-\vec{R})} W_n(\vec{r}-\vec{R}), \tag{7}$$

where $\vec{R}$ runs over the whole real-space lattice vectors. By substituting Eq. (7) into Eq. (2) and carrying out analytically the integral over $\vec{k}_\parallel$, it is straightforward to derive, for tetragonal perovskites, the polarization at individual $\vec{k}_\perp$ as

$$\phi(\vec{k}_\perp) = \frac{2\pi}{c}\sum_{\vec{R}_\perp}\sum_{n=1}^{M}\int \vec{r}_\parallel W_n^*(\vec{r}) W_n(\vec{r}-\vec{R}_\perp) e^{i\vec{k}_\perp\cdot\vec{R}_\perp} d\vec{r}, \tag{8}$$

where $\vec{r}_\parallel$ is the projection of vector $\vec{r}$ along the polarization direction and $\vec{R}_\perp$ is the projection of lattice vector $\vec{R}$ onto the plane perpendicular to the polarization direction. For convenience of discussion, we separate the sum over $\vec{R}_\perp$ into the $\vec{R}_\perp=0$ term and the rest,

$$\phi(\vec{k}_\perp) = \phi_0 + \frac{2\pi}{c}\sum_{\vec{R}_\perp\neq 0}\sum_{n=1}^{M}\int \vec{r}_\parallel W_n^*(\vec{r}) W_n(\vec{r}-\vec{R}_\perp) e^{i\vec{k}_\perp\cdot\vec{R}_\perp} d\vec{r}, \tag{9}$$

where for $\vec{R}_\perp=0$, $\phi_0=\Sigma_{n=1}^{M}\int(\vec{r})_\parallel W_n^*(\vec{r}) W_n(\vec{r}) d\vec{r}$ is the phase contribution from the same unit cell. Equation (9) is the basis for understanding the polarization structure. From this equation, we observe the following.

First, it is now clear that the $\vec{k}_\perp$-dependent part of $\phi(\vec{k}_\perp)$ comes only from the $\vec{R}_\perp\neq 0$ terms, which correspond to the overlap of the Wannier functions in neighboring cells. In other words, the $\vec{k}_\perp$ dependence of the $\phi(\vec{k}_\perp)$ phase results from the overlap of the Wannier functions of different cells that are displaced by $\vec{R}_\perp$ from each other within the plane that is perpendicular to the direction of polarization. While the choice of the Wannier function is known to be nonunique due to the gauge uncertainty, the sum of the Wannier-function overlap over occupied bands is a uniquely defined quantity which does not depend on the gauge. It is this quantity that determines the shape of the polarization structure.

Second, Eq. (9) explains why the bandwidth of polarization dispersion is often much smaller than 2π. Since only the second term in this equation is $\vec{k}_\perp$ dependent and since the Wannier functions are generally well localized compared to the size of unit cell, one expects the overlap $W_n^*(\vec{r})W_n(\vec{r}-\vec{R}_\perp)$ to be much smaller than unity for $\vec{R}_\perp \neq 0$. This is consistent with our numerical results in Fig. 1, namely, $\phi(\vec{k}_\perp)-\phi_0 \approx 0.6 \ll 2\pi$.

Third, since the dispersion in $\phi(\vec{k}_\perp)$ comes from the overlap of the Wannier functions between cells of different $\vec{R}_\perp$'s in the xy-in-plane directions, it explains why the polarization structure is very sensitive to in-plane strain, where by changing in-plane lattice constant, the distances between neighboring cells are effectively altered. Meanwhile, we recognize that a precise understanding of how the bandwidth depends on the in-plane strain is not as simple as one might think. Naively one tends to think that with the decline of in-plane lattice constant, the dispersion is to increase since the overlap $W_n^*(\vec{r})W_n(\vec{r}-\vec{R}_\perp)$ increases when $\vec{R}_\perp$ decreases. This will lead to the widening of the polarization-dispersion width, which is opposite to what we found in Fig. 3. This puzzling contradiction can be resolved by noticing that in addition to being dependent on the overlap strength between $W_n(\vec{r})$ and $W_n(\vec{r}-\vec{R}_\perp)$ within the perpendicular plane, the dispersion width also hinges on the localization length ($l_\parallel^{\mathrm{WF}}$) of the Wannier functions along the direction parallel to the polarization as a result of the $\vec{r}_\parallel$ operator in Eq. (9). With the increasing in-plane strain, the $l_\parallel^{\mathrm{WF}}$ is to shrink. We thus see that the bandwidth of polarization is determined by the balance of two competing factors between the increasing Wannier-function overlap and the decreasing $l_\parallel^{\mathrm{WF}}$ localization length. When the latter dominates, the bandwidth declines as we have seen in Fig. 3 from numerical calculations.

V. CURVE ANALYSIS

With the general understanding of the polarization structure in Sec. IV, we next attempt to determine analytically the polarization dispersion specifically for $PbTiO_3$, aiming to obtain further insight into the important details of the polarization structure. As will become clear later, our analysis in the following also explains what determines the $\phi(\vec{k}_\perp)$ polarization at special points of Γ, X_1, and X_2. We begin by defining parameters

$$t(\vec{R}_\perp) = \frac{2\pi}{c}\sum_{n=1}^{M}\int \vec{r}_\parallel W_n^*(\vec{r})W_n(\vec{r}-\vec{R}_\perp)d\vec{r}, \tag{10}$$

and then

$$\phi(\vec{k}_\perp) = \sum_{\vec{R}_\perp} t(\vec{R}_\perp)e^{i\vec{k}_\perp\cdot\vec{R}_\perp}. \tag{11}$$

For dielectrics of insulating nature, the Wannier functions are highly localized and decay exponentially with the distance.[21,22] As a result, $t(\vec{R}_\perp)$ also decay quickly with the increase in $|\vec{R}_\perp|$ so we can adopt the tight-binding-like approach and consider only several $\vec{R}_\perp$'s that correspond to some nearest neighbors (NNs). We consider up to the second NNs, where

$$\vec{R}_\perp = \begin{cases} (0\ \ 0) & \text{on site} \\ (\pm a\ \ 0) & \text{1NNs} \\ (0\ \ \pm a) & \text{1NNs} \\ (\pm a\ \ \pm a) & \text{2NNs.} \end{cases}$$

Taking advantage of tetragonal symmetry, we can rewrite Eq. (11) as

$$\phi(\vec{k}_\perp) = t_0 + 2t_1[\cos(k_1 a)+\cos(k_2 a)] + 2t_2[\cos(k_1+k_2)a+\cos(k_1-k_2)a], \tag{12}$$

where t_i is the ith NNs contribution defined in Eq. (10) and $\vec{k}_\perp=(k_1,k_2)$. This expression gives us a more direct sense of the $\phi(\vec{k}_\perp)\sim\vec{k}_\perp$ polarization dispersion, approximated to the second-nearest neighbors. At special $\vec{k}_\perp$ points of Γ, X_1, and X_2, the phases are $\phi(\Gamma)=t_0+4t_1+4t_2$, $\phi(X_1)=t_0-4t_2$, and $\phi(X_2)=t_0-4t_1+4t_2$, respectively. We could thus clearly see that the t_0 term, corresponding to $\vec{R}_\perp=0$, acts to rigidly shift the polarization curve as a whole. Meanwhile, the phase relative to the Γ (i.e., the dispersion) is determined by the t_1 and t_2 quantities and more specifically,

$$\phi(X_1)-\phi(\Gamma) = -4t_1 - 8t_2,$$

$$\phi(X_2)-\phi(\Gamma) = -8t_1. \tag{13}$$

These equations are useful since they tell us that (i) the relative height at X_2 (which contributes most to the polarization in PT), $\phi(X_2)-\phi(\Gamma)$, is determined by t_1, associated with the overlap of the Wannier function in the first NNs. $t_1<0$ for $PbTiO_3$ in equilibrium. (ii) Under the assumption that t_2 is negligible, $\phi(X_2)-\phi(\Gamma)$ will be larger than $\phi(X_1)-\phi(\Gamma)$ by a factor of 2.

Within the second-nearest-neighbor approximation, one can further determine analytically the dispersion along the $\Gamma\rightarrow X_1\rightarrow X_2\rightarrow\Gamma$ line in the 2D Brillouin zone as

$$\phi(\vec{k}_\perp) = \begin{cases} t_0+2t_1+(2t_1+4t_2)\cos(k_1 a) & \text{for } \Gamma\rightarrow X_1 \text{ with } k_2=0 \\ t_0-2t_1+(2t_1-4t_2)\cos(k_2 a) & \text{for } X_1\rightarrow X_2 \text{ with } k_1=\pi/a \\ t_0+2t_2+4t_1\cos(k_1 a)+2t_2\cos(2k_1 a) & \text{for } X_2\rightarrow\Gamma \text{ with } k_1=k_2. \end{cases}$$

TABLE I. The fitting t_1 and t_2 parameters for $PbTiO_3$ at different lattice constants. t_0 is not shown here since it does not affect dispersion.

a (Å)	t_1	t_2
3.88	−0.072	0.031
3.84	−0.072	0.032
3.80	−0.064	0.031
3.72	−0.031	0.023
3.65	−0.010	0.016

The polarization structure could thus be expressed as a simple combination of cosine functions.

To examine whether the second-NN approximation is sufficient, we fit the analytical results to the numerical DFT calculations to determine the t_i $(i=0,1,2)$ parameters. Note that only $\phi(\vec{k}_\perp)$'s at three points (i.e., Γ, X_1, and X_2) are fitted. The obtained t_i values are given in Table I. These values are then used to determine the whole dispersion curve, shown in Fig. 1(b) for $PbTiO_3$ in equilibrium structure of $a=3.88$ Å. We could see that the analytical curve agrees well with the DFT result, implying that the second-NN approximation works. On the other hand, some fine structure of the curve (such as the small local maximum along the Γ-X_1) cannot be reproduced, where for a better fitting, approximation beyond the second NNs would be necessary.

From Table I one can also see how the t_i quantities are influenced by in-plane strain. t_1 declines substantially as a decreases below 3.80 Å, while t_2 shows less dependence on in-plane strain. This makes sense since, by varying the in-plane strain, the main effect lies in altering the nearest-neighbor interaction among the Wannier functions. For $a>3.80$ Å, $|t_1|$ approximately equals $2|t_2|$, confirming the importance of the nearest-neighbor interaction. For large strains of $a<3.72$ Å, $|t_1|$ and $|t_2|$ become comparable, for which it is likely that higher orders of NNs are also needed.

VI. COMPARISON WITH BARIUM TITANATE

It is of interest to compare the polarization dispersions between $BaTiO_3$ (BT) and PT since these two substances have rather different tetragonality, magnitude of polarization, and sizes of A-site atoms. For this purpose, we have studied the polarization structure in BT, for which a tetragonal symmetry is enforced so that a direct comparison with PT can be made. Following the same procedure as for PT, we optimize the cell structure and atomic positions of BT at different in-plane lattice constants and calculate the corresponding polarization structures.

Figure 4 displays the polarization structure for $BaTiO_3$ at different in-plane lattice constants. Let us first focus on the dispersion of the equilibrium $BaTiO_3$. The LDA-calculated equilibrium in-plane lattice constant of BT is $a=3.95$ Å. Apart from similarities to PT (e.g., ϕ maximizes at X_2), our calculations reveal some interesting differences between PT and BT under zero strain. (i) The BT dispersion curve has a significantly smaller bandwidth (~0.42) than that of PT

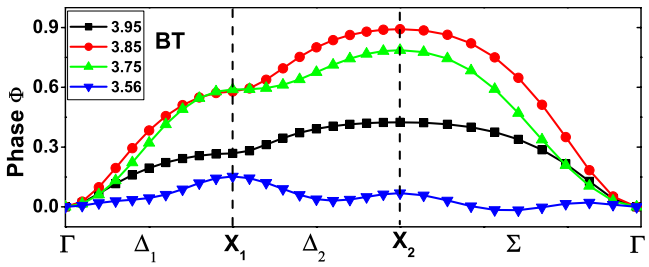

FIG. 4. (Color online) Polarization dispersions for $BaTiO_3$ at different in-plane lattice constants. Symbols are direct calculation results; lines are guide for the eyes.

(~0.57). Since the bandwidth is determined by the difference $\phi(X_2)-\phi(\Gamma)$, i.e., by t_1, a smaller bandwidth indicates less overlapping Wannier's functions between nearest neighbors in $BaTiO_3$, which could be explained by the larger in-plane lattice constant a for BT at equilibrium. (ii) Unlike PT, the polarization in BT is not small at X_1. This again can be attributed to the large in-plane lattice constant in BT, which leads to a negligible contribution from the second NNs, i.e., t_2 is small in BT. Indeed, we numerically found that t_2 is −0.007 in BT, compared to 0.031 in PT. By Eq. (13), $\phi(X_1)$ is about half of the $\phi(X_2)$ value if t_2 is small, which is indeed borne out in Fig. 4. (iii) As a consequence of observation (ii), the dispersions of BT and PT along the $\Gamma\rightarrow X_1$ are not quite similar. There is a local maximum between Γ-X_1 for PT, whereas for BT, no local maximum exists and X_1 becomes a saddle point.

Upon strain, $BaTiO_3$ and $PbTiO_3$ exhibit sharp difference in their strain dependence of dispersion bandwidth. As we saw previously in Fig. 3, in-plane strain causes the bandwidth declining for $PbTiO_3$. However, for $BaTiO_3$, a dramatic *enlargement* in bandwidth occurs when a decreases from 3.95 to 3.85 Å. The bandwidth maintains a large value at $a=3.75$ Å, after which it starts to drop. In $BaTiO_3$ the polarization-dispersion bandwidth thus shows an interesting nonmonotonous dependence on in-plane strain. This characteristic nonmonotonous dependence strongly supports our conjecture that the two competing factors determine the bandwidth, as described above in Sec. IV. When strain is small in BT, the overlapping of the Wannier functions located at the nearest-neighboring $\vec{R}_\perp$'s plays a dominant role, and the increasing overlap leads to a larger $|t_1|$ and thus larger bandwidth. As in-plane strain becomes large $(a<3.85$ Å), the atom-atom interaction along the c axis is considerably weakened due to elongated c-lattice length. As a consequence, the shrinking localization length $l_\parallel^{\mathrm{WF}}$ of Wannier functions along the $\vec{r}_\parallel$ direction takes over and becomes dominant, giving rise to the declining bandwidth. This, once again, reveals that the polarization dispersion contains rich information. To make more quantitative comparison, we replot in Fig. 5 the strain dependence of the $\phi(\vec{k}_\perp)$ phases at X_1 and X_2, relative to the Γ point. Figure 5 is of some useful value since it allows us to contrast the $\vec{k}_\perp$-specific polarizations in two materials at *the same* fixed in-plane lattice constant. The difference between BT and PT is thus not related in a significant sense to atom-atom distance but largely due to the overlap of respective Wannier's functions. In Fig. 5,

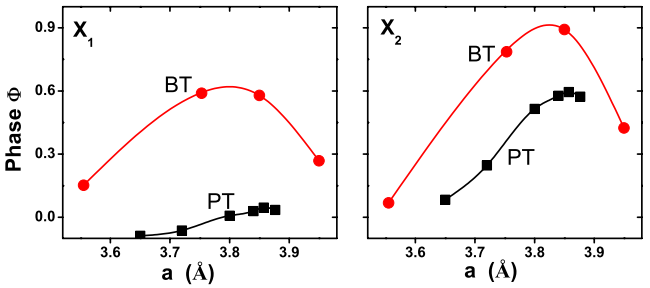

FIG. 5. (Color online) Dependencies of the $\phi(\vec{k}_\perp)$ phases at X_1 point (left) and at X_2 point (right) as a function of in-plane lattice constant for PT and BT.

both $\phi(X_1)$ and $\phi(X_2)$ are seen to be far greater in $BaTiO_3$ than in $PbTiO_3$ for a fixed a constant. The greater values of $\phi(\vec{k}_\perp)$ in BT could possibly originate from the fact that the Wannier functions in this material spread more due to the larger size of Ba atom.

From the comparison between PT and BT, we could see that the polarization structure has some common features for materials with similar structure and, meanwhile, some distinctions revealing the identities of materials. The common features allow us to understand the polarization structure in general; just as for band structure, most III-V semiconductors have direct band gaps. Differences in polarization structure manifest the electron wave functions and interatomic interactions on microscopic scale.

In addition to tetragonal phase, we also calculate the polarization structure in cubic perovskites (such as in $PbTiO_3$ and $BaTiO_3$ under high pressure). For cubic phase, the total polarization is null. In terms of the $\phi(\vec{k}_\perp)$ contribution at individual $\vec{k}_\perp$ point, there are two possible scenarios: one is that $\phi(\vec{k}_\perp)$ simultaneously vanishes at every $\vec{k}_\perp$ point and the other is that $\phi(\vec{k}_\perp)$ does not vanish individually but the total sum is null. Our calculation confirms the first scenario, i.e., $\phi(\vec{k}_\perp)$ is zero in cubic phase for all $\vec{k}_\perp$ points.

VII. SUMMARY

Two different approaches are employed to study the polarization structure in perovskite ferroelectrics. Numerically we use the density-functional total-energy calculations and the modern theory of polarization. Analytically we formulate a scheme to describe the $\vec{k}_\perp$ dependence of the polarization phase using the Wannier functions. By parametrizing the Wannier-function overlapping, we further identify the quantities that determine the $\phi(\vec{k}_\perp)$ phases at special $\vec{k}_\perp$ points of interest. Our specific findings are summarized in the following. For $PbTiO_3$ at equilibrium, (i) the $\phi(\vec{k}_\perp)$ phase maximizes at the Brillouin-zone boundary of the 2D $\vec{k}_\perp$ plane not the zone center. (ii) The polarization structure shows little dispersion along the Γ-X_1 line. However, the dispersion is large along the Γ-X_2. (iii) The bandwidth of the dispersion curve is far below 2π. The small dispersion considerably eases the difficulty in assigning the correct branch of individual $\vec{k}_\perp$ phase, but caution still needs to be taken when the $\phi(\vec{k}_\perp)$ phase is approaching 2π.

Analytically, (iv) expression (9) is given as the basis for understanding the polarization structure. It also explains why the polarization bandwidth is small compared to 2π. (v) The polarization phase at individual $\vec{k}_\perp$ is revealed to depend on the competition of two factors, namely, the overlapping strength of the Wannier functions within the perpendicular $\vec{R}_\perp$ plane and the localization length $l_\parallel^{\mathrm{WF}}$ of these Wannier functions. (vi) Within the 2NN approximation, the $\phi(X_1)$ and $\phi(X_2)$ values in ferroelectric perovskite are found to be $\phi(X_1)-\phi(\Gamma)=-4t_1-8t_2$, $\phi(X_2)-\phi(\Gamma)=-8t_1$. If t_2 is negligible, the latter is two times the former. (vii) When $PbTiO_3$ is under compressive in-plane strain, the polarization bandwidth is found to decrease, whereas the total polarization increases. The declining bandwidth implies that the localization length $l_\parallel^{\mathrm{WF}}$ of Wannier functions plays a dominating role in $PbTiO_3$.

By comparing $BaTiO_3$ with $PbTiO_3$, we show (viii) the equilibrium BT exhibits a smaller bandwidth of 0.42, as compared to the bandwidth of 0.57 in PT. (ix) $\phi(X_1)$ in $BaTiO_3$ is not small, unlike PT. The difference comes from the fact that t_2 is negligible in BT, leading to the result that $\phi(X_1)$ is about half of the value of $\phi(X_2)$. But in PT, t_2 cannot be neglected and acts to offset the t_1 contribution, giving rise to smaller $\phi(X_1)$ and flat dispersion along the Γ-X_1 line. (x) As $BaTiO_3$ is under increasing in-plane strains, its polarization bandwidth displays a characteristic nonmonotonous variation by first increasing dramatically and then declining. The finding lends a support to the qualitative understanding that two competing factors determine the $\phi(\vec{k}_\perp)$ phase. (xi) When $BaTiO_3$ and $PbTiO_3$ are constrained to the same in-plane lattice constant, the $\phi(X_1)$ and $\phi(X_2)$ are shown to be significantly larger in BT than in PT, unlike the case when two materials are in equilibrium.

We conclude by pointing out that there are still many aspects of polarization structure we do not yet understand. For example, we have not pursued beyond the second-nearest neighbors to explain the local maximum between Γ and X_1 in unstrained PT. We also do not know the physical significance when $\phi(X_1)$ changes from a local minimum to a saddle point as displayed in Fig. 3 for $PbTiO_3$ under strains. We believe that further analysis of the polarization structure could yield better knowledge on the physics of dielectrics. Like band structure of solids, we hope that the polarization structure can provide us a new tool of studying ferroelectric materials and properties.

ACKNOWLEDGMENT

This work was supported by the Office of Naval Research.

[1] M. E. Lines and A. M. Glass, *Principles and Applications of Ferroelectrics and Related Materials* (Clarendon, Oxford, 1979).
[2] I. Souza, J. Iniguez, and D. Vanderbilt, Phys. Rev. Lett. **89**, 117602 (2002).
[3] P. Umari and A. Pasquarello, Phys. Rev. Lett. **89**, 157602 (2002).
[4] H. Fu and L. Bellaiche, Phys. Rev. Lett. **91**, 057601 (2003).
[5] O. Dieguez and D. Vanderbilt, Phys. Rev. Lett. **96**, 056401 (2006).
[6] R. D. King-Smith and D. Vanderbilt, Phys. Rev. B **47**, 1651 (1993).
[7] R. Resta, Rev. Mod. Phys. **66**, 899 (1994).
[8] H. J. Monkhorst and J. D. Pack, Phys. Rev. B **13**, 5188 (1976).
[9] P. Y. Yu and M. Cardona, *Fundamentals of Semiconductors* (Springer, Berlin, 2001).
[10] K. J. Choi, M. Biegalski, Y. L. Li, A. Sharan, J. Schubert, R. Uecker, P. Reiche, Y. B. Chen, X. Q. Pan, V. Gopalan, L.-Q. Chen, D. G. Schlom, and C. B. Eom, Science **306**, 1005 (2004).
[11] J. H. Haeni, P. Irvin, W. Chang, R. Uecker, P. Reiche, Y. L. Li, S. Choudhury, W. Tian, M. E. Hawley, B. Craigo, A. K. Tagantsev, X. Q. Pan, S. K. Streiffer, L. Q. Chen, S. W. Kirchoefer, J. Levy, and D. G. Schlom, Nature (London) **430**, 758 (2004).
[12] C. Ederer and N. A. Spaldin, Phys. Rev. Lett. **95**, 257601 (2005).
[13] H. N. Lee, S. M. Nakhmanson, M. F. Chisholm, H. M. Christen, K. M. Rabe, and D. Vanderbilt, Phys. Rev. Lett. **98**, 217602 (2007).
[14] H. W. Jang, S. H. Baek, D. Ortiz, C. M. Folkman, R. R. Das, Y. H. Chu, P. Shafer, J. X. Zhang, S. Choudhury, V. Vaithyanathan, Y. B. Chen, D. A. Felker, M. D. Biegalski, M. S. Rzchowski, X. Q. Pan, D. G. Schlom, L. Q. Chen, R. Ramesh, and C. B. Eom, Phys. Rev. Lett. **101**, 107602 (2008).
[15] P. Hohenberg and W. Kohn, Phys. Rev. **136**, B864 (1964); W. Kohn and L. J. Sham, *ibid.* **140**, A1133 (1965).
[16] H. Fu and O. Gulseren, Phys. Rev. B **66**, 214114 (2002).
[17] N. Troullier and J. L. Martins, Phys. Rev. B **43**, 1993 (1991).
[18] Details were given in Ref. 16 and in Z. Alahmed and H. Fu, Phys. Rev. B **76**, 224101 (2007).
[19] X. Wu, O. Dieguez, K. M. Rabe, and D. Vanderbilt, Phys. Rev. Lett. **97**, 107602 (2006).
[20] M. Stengel and N. A. Spaldin, Phys. Rev. B **75**, 205121 (2007).
[21] J. Des Cloizeaux, Phys. Rev. **135**, A698 (1964).
[22] N. Marzari and D. Vanderbilt, Phys. Rev. B **56**, 12847 (1997).